
Article:
Zhu, J., Pugh, S. and Dwyer-Joyce, R.S. orcid.org/0000-0001-8481-2708 (2012) Model and experiments to determine lubricant film formation and frictional torque in aircraft landing gear pin joints. Proceedings of the Institution of Mechanical Engineers, Part J: Journal of Engineering Tribology, 226 (4). pp. 315-327. ISSN 1350-6501

https://doi.org/10.1177/1350650111434247

Model and Experiments to Determine Lubricant Film Formation and Frictional Torque in Aircraft Landing Gear Pin Joints

J. Zhu, S. Pugh, R.S. Dwyer-Joyce

Leonardo Centre for Tribology, Department of Mechanical Engineering, the University of Sheffield, Mappin Street, Sheffield, S1 3JD

Abstract

Pin joints are found in many large articulating structures. They tend to be under high load and articulate slowly, so the joints typically operate in the boundary or mixed lubrication regimes. This means that the operating torque depends on the respective proportions of liquid and solid contact between the joint mating faces. In this paper, a mixed lubrication model of a grease lubricated landing gear joint is established to determine a theoretical Stribeck curve, frictional torque and lubricant film thickness under different loads. Parameters describing pin joint working conditions, geometry, lubricant properties and pin/bush texture are used. The model can also predict the proportion of the load that is supported by contacting asperities and lubricant film. The changing proportions of these two parts indicate transformations between different lubrication regimes. Experiments on an instrumented pin joint have been carried out to compare with the predicted friction and torque performance. Theoretical calculation results show good consistency with experimental plots at high load. But under low load the real friction between pin and bush is significantly lower than theoretical predictions.

Keywords: landing gear pin joint, mixed lubrication model, friction coefficient, frictional torque, film thickness

1. Introduction

Pin joints allow mechanical articulation between two or more members in a structure. They are widely used in many kinds of engineering machinery, from heavy mining equipment to the latest evolution of the space shuttle. They play a key role in the operation and durability of articulating mechanisms.

A typical example is that of aircraft landing gear (see Figure 1). Articulation in landing gear systems is achieved by using of many pin joints, which help to complete the extending and retracting movement. The joints consist of a hollow steel pin that is

free to reciprocate inside aluminium bronze bushes. The bushes are press fitted into the landing gear members. The joints are lubricated by grease which is replenished manually at regular maintenance intervals. The lubricant film formed separates the surfaces of the pin and bush and reduces metallic contact and wear. Ideally this lubricant film should be as thick as possible to minimise solid contact and therefore friction. Lower friction force ultimately means that smaller actuators are possible, therefore saving weight.

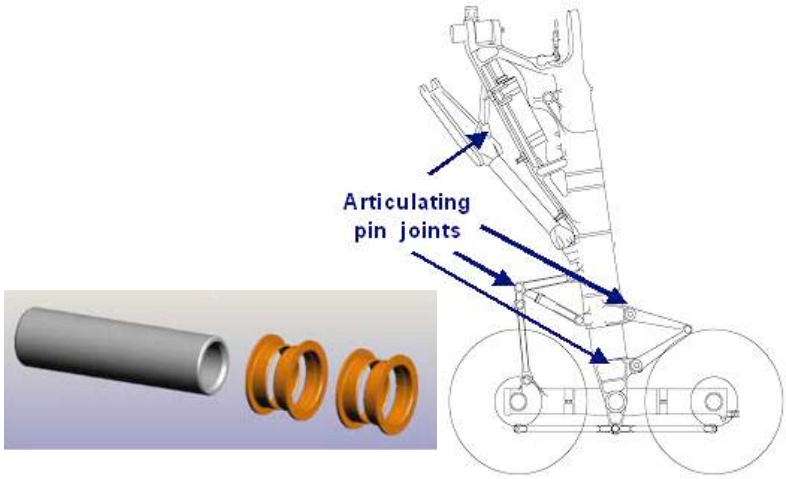

Figure 1 Sketch of landing gear and typical pin joint

The landing gear joints oscillate under low-speed and heavy-load conditions. The pin joints are therefore operating in boundary or mixed lubrication regime. Much experimental work on bearing material selection and wear for these kinds of joints has been done [1, 2]. The results show bearing performance effectively and give some beneficial instructions for bearing design. But there are still no theories available to predict friction coefficient accurately for low-velocity, high-load and articulating bearings.

In this paper, a mixed lubrication model of a grease lubricated pin joint is used to predict lubrication regimes and joint friction coefficient. A test rig has been used to articulate a sample pin joint with full instrumentation. The torque required is then compared with theoretical results.

2. Model Formulation

This model follows a similar approach to Lu etc al [3] where friction coefficient is predicted as the sum of the friction at the dry asperity contacts and viscous friction from the fluid film parts. An equation for asperity contact is based on the Greenwood

& Williamson [4] model; while another equation for the fluid film determined by the Moes's method [5].

2.1 Friction coefficient in mixed lubrication

In the mixed lubrication model of Johnson et al [6] the total normal load P_T is shared by the hydrodynamic lifting force P_H and the asperity contact force P_C.

$$P_T = P_H + P_C \tag{1}$$

Correspondingly the friction force Q_T is composed of two parts, one is hydrodynamic friction force Q_H that mostly relies on lubricant viscosity and the other is asperity interacting shear stress, Q_C , which is influenced mainly by the morphology of the mating surfaces. Figure 2 shows the load distribution in mixed lubrication regime.

$$Q_T = Q_H + Q_C \tag{2}$$

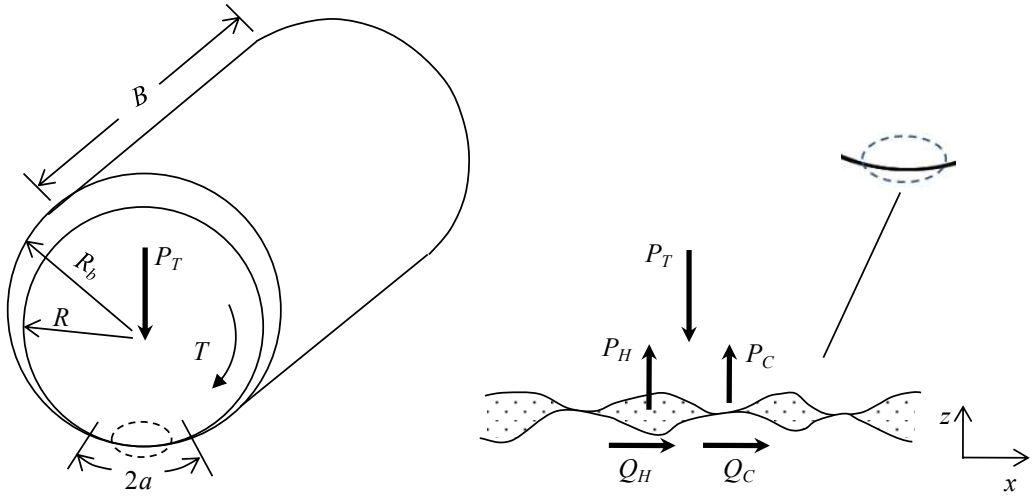

Figure 2 Schematic diagram of pin joint and load distribution in the mixed lubrication contact

The frictional force caused by the hydrodynamic fluid film, Q_H , is derived from Bair-Winer model [7]

$$Q_H = \tau_L \left(1 - e^{-\eta u / \tau_L h_c}\right) 2aB \tag{3}$$

where τ_L is the limiting shear stress, η is lubricant viscosity which is assumed to obey the Roelands' equation[8], u is the effective velocity of contacting surfaces, h_c is the central film thickness, a is the half width of Hertzian contact, B is the bush length of

the pin joint. Both the parameters τ_L and η are functions of the pressure in the contact, p_m, according to:

$$\tau_L = \tau_{L0} + \beta_0 p_m \tag{4}$$

$$\eta = \eta_0 \left(\eta_\infty / \eta_0\right)^{\left[1-\left(1+p_m/c_p\right)^Z\right]} \tag{5}$$

with τ_{L0} is the limiting shear stress at ambient pressure, β_0 is the slope of the limiting shear stress-pressure relation, η_0 is the lubricant viscosity at inlet temperature, η_∞ and c_p are constants, Z is the Roelands' pressure-viscosity index.

To simplify the model in this work the contact between the pin and bush is assumed to follow Hertz elastic contact analysis. Strictly this kind of contact violates the Hertz principle because the contact area is not small compared with the radius of the contacting bodies. However, an experimental analysis [9] shows that the approximation is not too severe. The mean and peak contact pressures and half contact width are then given by:

$$p_m = \frac{P_T}{2aB}, p_0 = \sqrt{\frac{P_T E^{'}}{2\pi B R^{'}}}, a = \sqrt{\frac{8 P_T R^{'}}{\pi E^{'} B}} \tag{6}$$

where R' is the reduced radius

$$\frac{1}{R^{'}} = \frac{1}{R} - \frac{1}{R_b}$$

Where R and R_b are the outer radius of pin and inner radius of bush respectively, and E' is the effective modulus

$$\frac{1}{E^{'}} = \frac{1}{2}\left(\frac{1-\nu_b^{\,2}}{E_b} - \frac{1-\nu^2}{E}\right)$$

The friction caused by the asperity contacts, Q_C, is expressed by [3]:

$$Q_C = \sum_{1}^{i=N} \mu_{Ci} p_{Ci} dA_{Ci} \tag{7}$$

with μ_{Ci}, p_{Ci}, dA_{Ci} refer to the friction coefficient, mean contact pressure, and area of contact at a pair of contacting asperities, i. N is the total number of asperity contact points. If the friction coefficient, Q_C is assumed to be constant over all asperity contacts, then

$$Q_C = \mu_C \sum_{1}^{i=N} p_{Ci} dA_{Ci}$$
$$Q_C = \mu_C P_C \tag{8}$$

γ_1 and γ_2 were introduced in Johnson's model [6] to represent the proportions of hydrodynamic lifting force and surface asperity contacting pressure. They are written as $\gamma_1 P_H = P_T, \gamma_2 P_C = P_T$. Together with equation(1), then:

$$\frac{1}{\gamma_1} + \frac{1}{\gamma_2} = 1 \tag{9}$$

The friction coefficient for pin / bush contact is obtained from:

$$\mu = \frac{Q_H + Q_C}{P_T} \tag{10}$$

The frictional torque to rotate the pin joint is then:

$$T = \mu R P_T \tag{11}$$

Note that equation (11) in fact represents an approximation for the torque from the pressure distribution. Ref [9, 10] describe in detail how the tangential pressure components reduce this torque. However, the effect is relatively small (leading to a reduction of less than 10%) and so for simplicity is neglected here.

In order to determine the friction coefficient using equation (10) the film thickness and proportions of liquid and solid contact are needed. One approach of doing this has been developed by Lu et al [3] and Gelinck & Schipper [11], who set up a mixed lubrication model to calculate Stribeck curves for line contacts. In this paper, this model was chosen to establish a friction and lubrication model for the pin joint. As in the mixed lubrication regime both elastohydrodynamic lubrication (EHL) and asperity contact exist to support the total load. So in this lubrication model the elastohydrodynamic lubrication theory and rough surface contact theory are needed. The following part explains this mixed lubrication model.

2.2 Elastohydrodynamic lubrication component

The approach [3, 11] assumes the formation of the oil film is unaffected by the presence of the roughness. Then a conventional smooth surface EHL solution is used to determine the load supported by the hydrodynamic film.

In the present case, the Moes [5] equation was used to predict the central film thickness in the line contact:

$$H_C = \left[\left(H_{RI}^{7/3} + H_{EI}^{7/3} \right)^{3s/7} + \left(H_{RP}^{-7/2} + H_{EP}^{-7/2} \right)^{-2s/7} \right]^{1/s} \tag{12}$$

where the dimensionless parameters are defined as follows:

$$s = \frac{1}{5}\left(7 + 8e^{\left(-2\frac{H_{EI}}{H_{RI}} \right)} \right),$$
$$H_{RI} = 3M^{-1}, H_{EI} = 2.621M^{-1/5},$$
$$H_{RP} = 1.287L^{2/3}, H_{EP} = 1.311M^{-1/8}L^{3/4},$$
$$H_C = \frac{h_c}{R'}U_\Sigma^{-1/2}, M = WU_\Sigma^{-1/2}, L = GU_\Sigma^{1/4}$$
$$W = \frac{P_T}{E'R'B}, U_\Sigma = \frac{\eta_0 u}{E'R'}, G = \alpha E'.$$

where h_c is the separation in the center of the contact, H_C are dimensionless film thicknesses, U_Σ is the dimensionless viscosity, M and W are dimensionless load parameters, L and G are material parameters, α is the pressure-viscosity coefficient.

According to Gelink and Schipper [11] the hydrodynamic part of the mixed lubrication is considered in equation (12) by replacing E' with E'/γ_1 and P_T with P_T/γ_1. So the film thickness equation (12) can be rewritten by:

$$\frac{h_c}{R'}U_\Sigma^{-1/2} = \left[(\gamma_1)^{s/2} \left(H_{RI}^{7/3} + (\gamma_1)^{-14/15} H_{EI}^{7/3} \right)^{3s/7} + (\gamma_1)^{-s/2} \left(H_{RP}^{-7/2} + H_{EP}^{-7/2} \right)^{-2s/7} \right]^{1/s} (\gamma_1)^{1/2} \tag{13}$$

with s is expressed as:

$$s = \frac{1}{5}\left(7 + 8e^{\left(\left(-2\frac{H_{EI}}{H_{RI}} \right)\gamma_1^{-2/5} \right)} \right) \tag{14}$$

2.3 Asperity contact component

The rough surface contacting model of Greenwood and Williamson [4] is used to determine the load supported by the asperity contact part. The pressure generated by the asperity contact is given by,

$$p(x) = \frac{2}{3} n\beta^{1/2} \sigma_s^{3/2} E' F_{3/2}\left(\frac{h(x)}{\sigma_s}\right) \tag{15}$$

where h is the separation between the two contacting surfaces, n is the density of the asperities, β is the average radius of the asperities, σ_s is the standard deviation of the height distribution of the summits. $F_{3/2}\left(\frac{h(x)}{\sigma_s}\right)$ is expressed as,

$$F_{3/2}\left(\frac{h(x)}{\sigma_s}\right) = \frac{1}{\sqrt{2\pi}} \int_{h(x)/\sigma_s}^{\infty} \left(t - \frac{h(x)}{\sigma_s}\right)^{3/2} e^{-t^2/2} dt \tag{16}$$

So the central contact pressure can be expressed by:

$$p_c = \frac{2}{3} n\beta^{1/2} \sigma_s^{3/2} E' F_{3/2}\left(\frac{h_c - d_d}{\sigma_s}\right) \tag{17}$$

where d_d is the distance between the mean plane through the summits and the mean plane through the surface heights. According to Whitehouse and Archard [12] d_d is approximately $1.15\sigma_s$. The expression for the statistical function $F_{3/2}$ depends on the distribution of asperity heights $\emptyset(z)$ [4], which is usually modeled as Gaussian distribution.

Gelinck and Schipper [11] fitted the following expression for the central pressure,

$$p_c = p_0 \left[1 + \left(a_1 n^{a_2} R'^{3a_2/2 - a_3} \beta^{a_2/2} \sigma_s^{a_3} W^{a_2 - a_3}\right)^{a_4}\right]^{1/a_4} \tag{18}$$

with $a_1 = 1.558$, $a_2 = 0.0337$, $a_3 = -0.442$, $a_4 = -1.7$, p_0 is the maximum Hertzian pressure determined from an elastic smooth line contact, which is given by equation (6).

Combining equation (17) and (18), substituting E'/γ_2 for E', P_T/γ_2 for P_T, and $n\gamma_2$ for n, gives the relationship between the surface roughness parameters, the geometry of the pin joint contact, the applied load and the separating film thickness:

$$\begin{aligned} &\frac{2\sqrt{2\pi}}{3}\left(\frac{BR'E'}{P_T}\right)^{1/2} n\beta^{1/2}\sigma_s^{3/2} F_{3/2}\left(\frac{h_c - d_d}{\sigma_s}\right) \\ &= \frac{1}{\gamma_2}\left[1 + \left(a_1 n^{a_2} R'^{3a_2/2 - a_3} \beta^{\frac{a_2}{2}} \sigma_s^{a_3} W^{a_2 - a_3} \gamma_2^{a_2}\right)^{a_4}\right]^{1/a_4} \end{aligned} \tag{19}$$

3 Numerical simulation for a pin-joint

3.1 Input parameters

The set of equations (9), (13), and (19) have three unknown parameters: γ_1, γ_2 and h_c which define the relative proportions of liquid and solid contact. A MathCAD program was written to solve this set of simultaneous equations for given input conditions. Once the film thickness and load sharing are known, the friction coefficient can be solved from equations(3), (8) and(10). Equation (11) is then used to calculate frictional toque.

The pin being modelled is a high strength corrosive resistant steel (300M) while the four bushes are made of aluminium bronze. They are machined with high-quality ground surface finish. Characteristics and operating conditions of the pin joint are shown in Table 1.

Table 1 Characteristics and operating conditions of pin joint

Symbol	Parameter	Value
E	elastic modulus of pin	205GPa
E_b	elastic modulus of bush	117GPa
ν	Poisson's ratio of pin	0.28
ν_b	Poisson's ratio of bush	0.34
R	radius of pin	28mm
R_b	radius of bush	28.025mm
B	length of bush	59.4mm
P_T	total normal load	5,10,20,40,60 kN
c	radial clearance	25μm
f	rotation frequency of pin	0.03Hz, 0.3Hz, 1Hz

The surface roughness parameters for the pin and bush contact faces were measured using a stylus profilometer. Sample length of 4mm along axial direction for pin and bush were measured. Each measurement was carried out three times and the mean value was adopted. All the parameters are shown in Table 2. For n, β and σ_s, the

combined values for the two surfaces are used. They are expressed as the average of pin and bush.

Table 2 Surface parameters of pin joint

Symbol	Parameter	Value
n	density of asperities	7.15×10^{9} m^{-2}
β	average asperity radius	3.4 μm
σ_s	standard deviation of asperity height	1.09 μm
σ	root mean square roughness of pin	0.83 μm
σ_b	root mean square roughness of bush	1.35 μm
d_d	distance between the mean plane through the summits and the mean plane through the surface heights	1.25 μm

In this paper Aeroshell 33 was used to lubricate pin joint. The relevant properties in this lubrication model are shown in Table 3.

Table 3 Parameters of lubricant

Symbol	Parameter	Value
β_0	slope of the limiting shear stress-pressure relation[13]	0.047
τ_{L0}	limiting shear stress at ambient pressure[13]	2.28×106 Pa
η_0	lubricant viscosity at inlet temperature	12.45×10^{-3} Pa·s
η_∞	constant in Roelands's formula[8]	6.31×10^{-5} Pa·s
c_p	constant in Roelands's formula[8]	1.96×10^{8} Pa
Z	Roelands' pressure-viscosity index[8]	0.63
α	pressure-viscosity coefficient	16.9 GPa^{-1}

A critical unknown in this model is the "dry" friction coefficient, μ_C, that exists between the two solid surfaces at the asperity contact points. This parameter is very difficult to predict and can only be determined by experiment. In the absence of any data for this parameter, a value of 0.12 has been used in this work. The selection of this value is somewhat arbitrary. It is difficult to know exactly the nature of the conditions are at the asperity to asperity contacts. A surface coated with anti-wear or

extreme pressure additive would have a friction coefficient in this area [14]. Other authors [11] use a similar value.

3.2 Theoretical prediction of friction coefficient and film thickness

Under varying pin joint operating conditions, numerical solutions for friction coefficient, film thickness, lambda ratio and the scaling factors have been obtained.

Figure 3 shows the predicted scaling factors and friction coefficient variation with the pin joint operating conditions. The pin joint duty is expressed in terms of the Sommerfeld number defined as [15]:

$$S = \frac{\eta\omega}{2\pi P_L}\left(\frac{R}{c}\right)^2 \tag{20}$$

As the Sommerfeld number increases (by the joint articulation velocity increasing) more lubricant is dragged into pin joint contact to maintain the pressure field. This causes the increasing film thickness and can be seen in Figure 3 as $1/\gamma_1$ becomes greater. This process agrees with the theory that pressure magnitudes are proportional to the square of the reciprocal of film thickness [16]. When the lubricant film supports most of the load, contact between asperities declines. The composite result is that friction coefficient of pin/bush contacting decreases with Sommerfeld number.

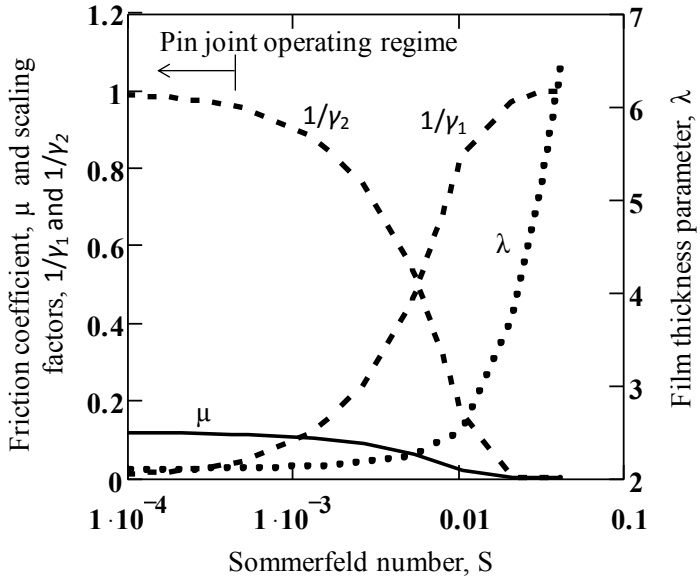

Figure 3 Friction coefficient, scaling factors and film thickness parameter plotted against Sommerfeld number for a pin joint load of 20kN

Also shown on Figure 3 is the lambda ratio, λ, where:

$$\lambda = h_{\min} / \sqrt{\sigma_b{}^2 + \sigma^2} \tag{21}$$

In the simulation work carried out in this study, the pin joint speed has been set in the range 1 to 800 rpm under pressures from 7 to 23MPa. This results in Sommerfeld number in the range 0 to 0.15. For the load of 20 kN (13MPa), This range is marked in figure 3 clearly shows that the dominant mechanism is one of solid contact and hydrodynamic film formation plays little part in influencing friction.

Figure 4 shows maps of the friction coefficient and lambda ratio determined from the model for various pin joint loads and speeds. Again the operating region for the pin joint is shown. The data indicates that friction coefficients do not fall below 0.11 as lambda ratios stay below 2. Clearly in this region of operation the prediction friction coefficient is highly depends on the value selected for the dry friction coefficient, μ_C. This is in common with many other models of mixed lubrication, is a limitation of the approach.

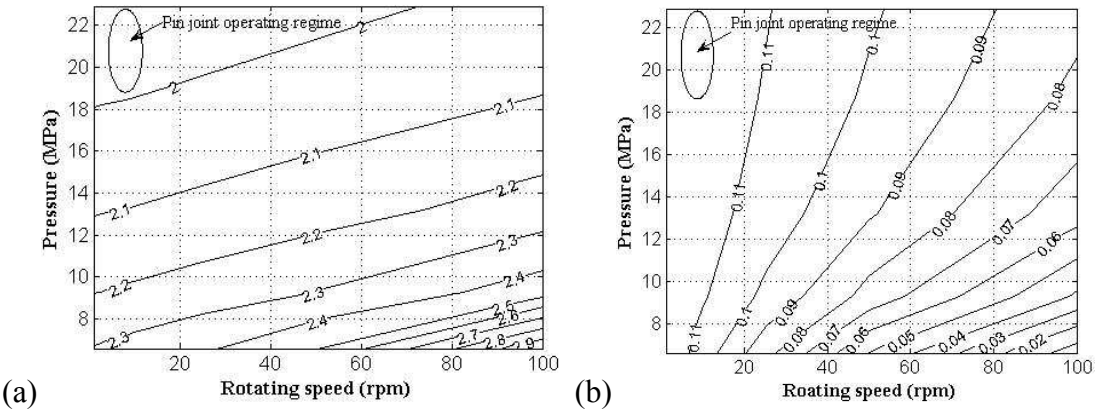

(a) (b)

Figure 4 Maps of pin joint operation (a)lambda ratio, (b)friction coefficient

4. Experimental Apparatus

4.1 Pin joint function tester

A double fork arrangement is used to load and support the pin within the test bushes (see Figure 5). The inner fork has four bushes press fitted. The outer fork has two rolling bearings as shown. A low height hydraulic cylinder is then used to load the two forks apart. This double arrangement is geometrically similar to the pin joint arrangement found on the landing gear upper to lower side-stay pin. This housing was then mounted on a torsional servo-hydraulic actuator. Four slots shown by a sketch in Figure 6 and the photo in Figure 5 were wire cut at one end, which enabled a direct

line axial coupling via a splined interface to the torsion drive shaft. The right photo of Figure 5 shows the double forks head assembled onto the torsional actuator.

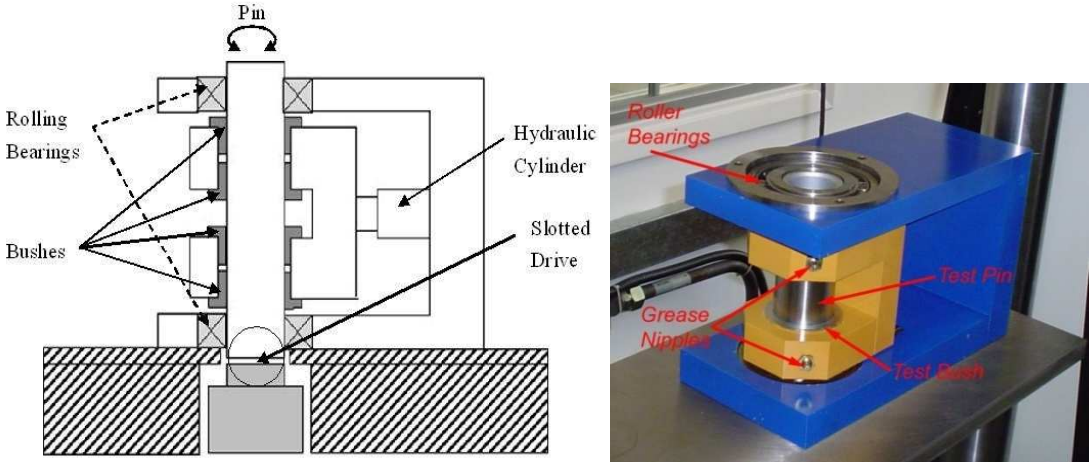

Figure 5 Sketch and photograph of pin joint test apparatus

4.2 Pin and Bush Specimens

A pin and four bushes were obtained from an actual upper to lower side-stay pin joint and were used as the test specimens, shown in Figure 6. The single pin, OD 56mm, ID42±0.2mm, length 200.5±0.1mm mated with four bushes with the radial clearance of 25μm. The four aluminium bronze bushes have an inner diameter ID of 56mm. Aeroshell 33 was applied and operated with two axial lubrication grooves in the bush. The grease was fed to the contact by means of channels and grease nipples, shown in Figure 5.

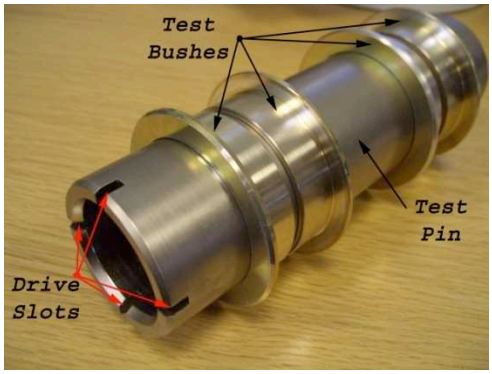

Figure 6 Photograph of the pin and bush system

4.3 Instrumentation

The servo-hydraulic torsional actuator was fitted with both an angular position sensor and a strain gauge based internal torque sensor. The tension hydraulic actuator could

be driven in both torque and angular displacement control. For all work in this paper only displacement control was used via angular control from a function generator. The reacted torque was then recorded during the cycle.

The torque transducer will also measure the torque in the two support rolling bearings. However this torque is low compared with the torque from the pin joints. The torque in the ball bearings was measured when unloaded (i.e. the pin not in place) and found to be within the noise range of the transducer.

The overall monitoring, recording and control of the rig was via a PC using a software program written in Labtech Notebook. During testing the duration of each test, the angular position of pin relative to the start position and the frictional torque were recorded. Figure 7 (a) shows the response of the angular displacement sensor for one complete cycle. The rotation is a smooth and continuous sine wave. Recording position data are then inputted in MathCAD to deduce the velocity characteristic curve which is an important parameter in determining friction coefficient. This is shown in Figure 7 (b). The frictional torque was also recorded throughout the cycle. Figure 7 (c) and (d) show this plotted against time and articulation angle respectively.

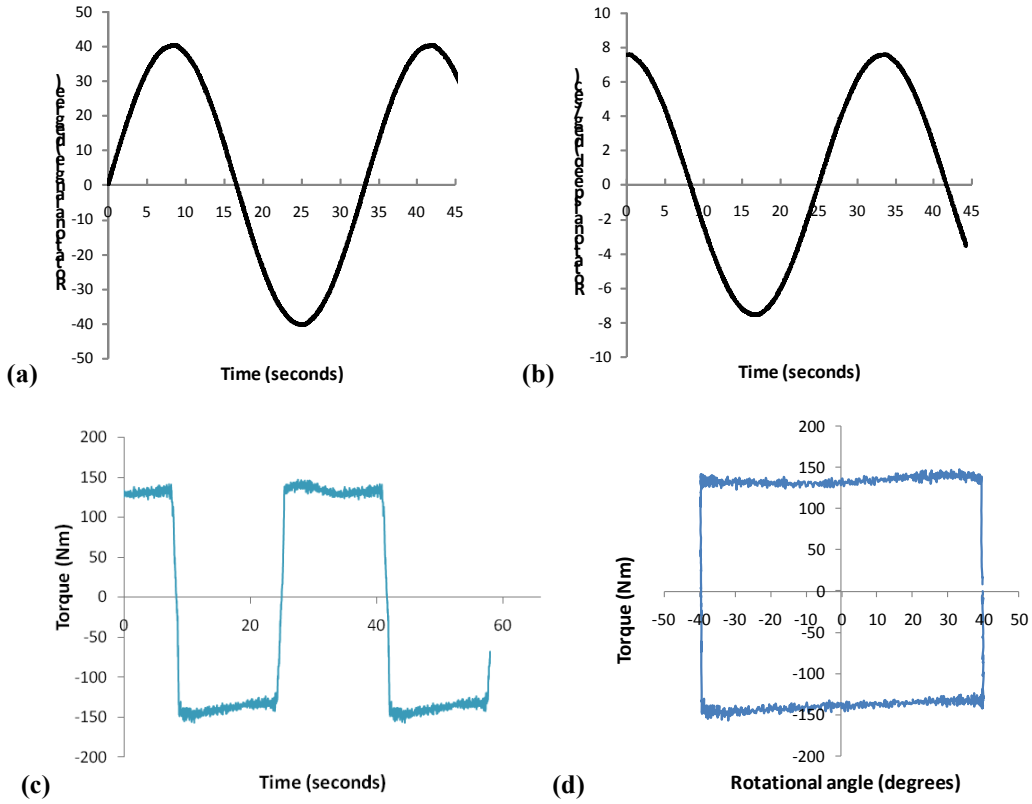

Figure 7 Typical data recorded by the pin joint apparatus

(a)the angular displacement, (b)the rotational speed, (c)the torque plotted against time, and (d)the torque plotted against rotational angle

At the start and stop points, where the speed is zero, the recorded torque is slightly higher. The torque drops then during the articulation, reaches a minimum at around zero degree, and rises again towards the next peak. This demonstrates that the torque reduces as the pin joint speed increases. The sliding motion between pin and bush entrains some grease and generates a thin lubrication film, which leads to the torque reduction.

Thermocouples were imbedded in the housing close to the location of the bushes. Temperature was monitored throughout testing. However, the tests presented here were short duration (a few cycles) and so significant heating above room temperature did not occur.

4.4 Operating Conditions

The tests were carried out fully greased with a range of radial load, (from 5 to 60 kN). The torsional actuator had a maximum capacity of 200 Nm. The maximum radial load achievable on the pin is therefore a function of the friction coefficient between the pin and bush. The typical rotational speed of pin joint is 0.033 Hz, (12 deg/s; equalled to the actual main lock stay articulation speed). In this research, experiments at different frequencies of 0.03 Hz, 0.3 Hz and 1 Hz were done with pin angular displacement of ±40°.

5. Comparison of Simulation and Experiment

The average torque during each complete articulation was used for calculating the friction coefficient from equation(11). The friction coefficient was then plotted against Sommerfeld number, rotation speed and load respectively shown by Figure 8 to Figure 10. Comparing with simulation results it is apparent that pin joint is working in boundary lubrication regime on most occasions. The higher load cases show close agreement between model and experiment. The friction coefficient for low speed when there is negligible hydrodynamic lift is 0.117 which is close to the value of $\mu_C = 0.12$ that was assumed in the modeling. However at lower load the agreement is not so good. The onset of fluid film formation appears to be occurring at lower speed. It is possible that at these lower loads the grease is not being squeezed out of the

contact as effectively as at the higher loads. And also grease thickeners improve the friction property of pin joint because of the formation of films on the surface of the metal. This may result in improved film formation.

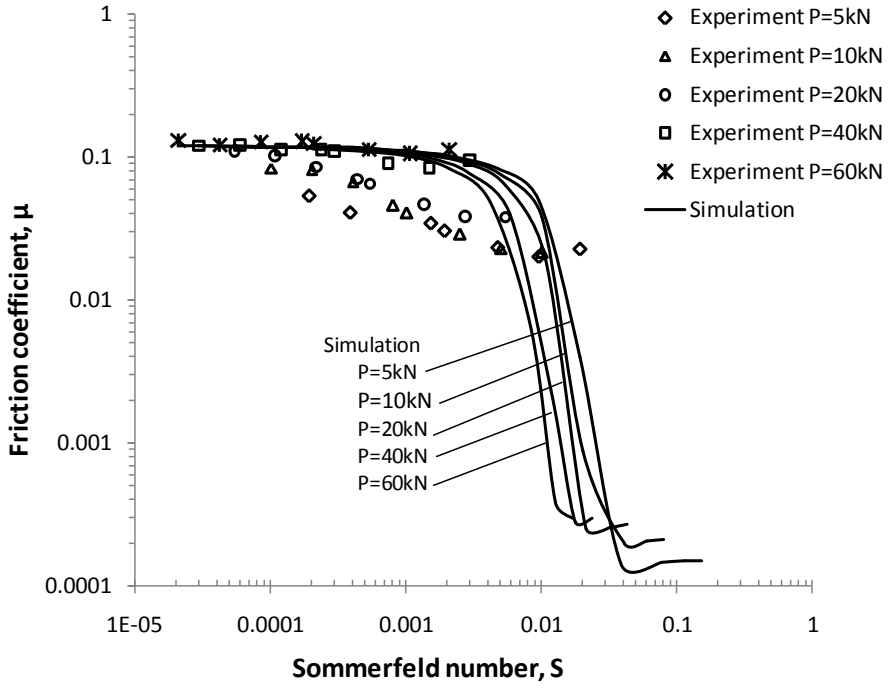

Figure 8 Friction coefficient vs Sommerfeld number with varying load

The influence of pressure and velocity on friction is expressed in Figure 9 and Figure 10. Model predictions and experimental results show acceptable agreement. However the comparison indicated by Figure 9 demonstrates that the effect of load is more pronounced that would be expressed by the theory. The simulation assumes the contact is fully flooded. In reality the joint articulating and the high load squeezes grease out of the contact. The greater the load & the lower reciprocation frequency the harder it is for the grease to flow back. This may be the reason why the higher loads show a higher friction coefficient.

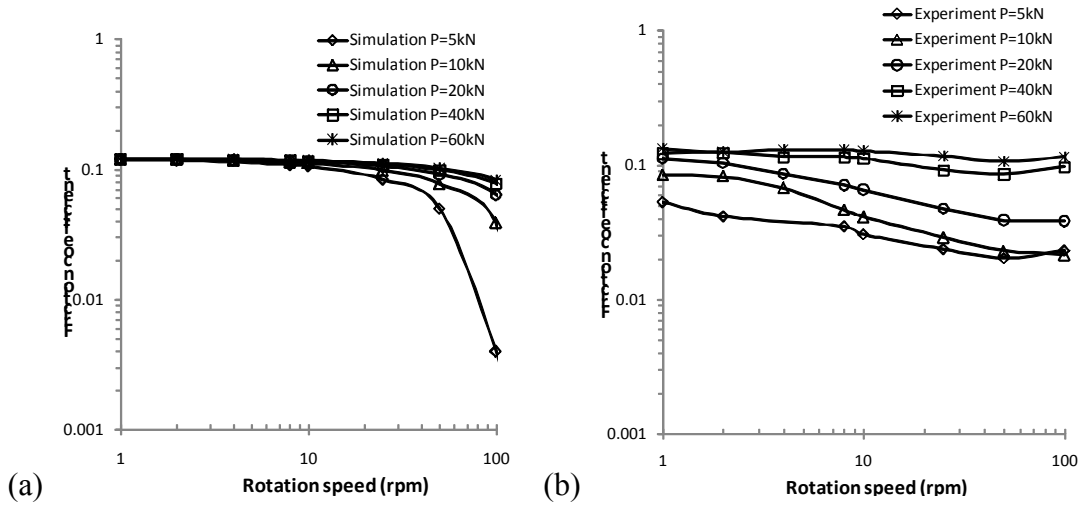

Figure 9 Friction coefficient against sliding speed (a) simulation, (b) experiment

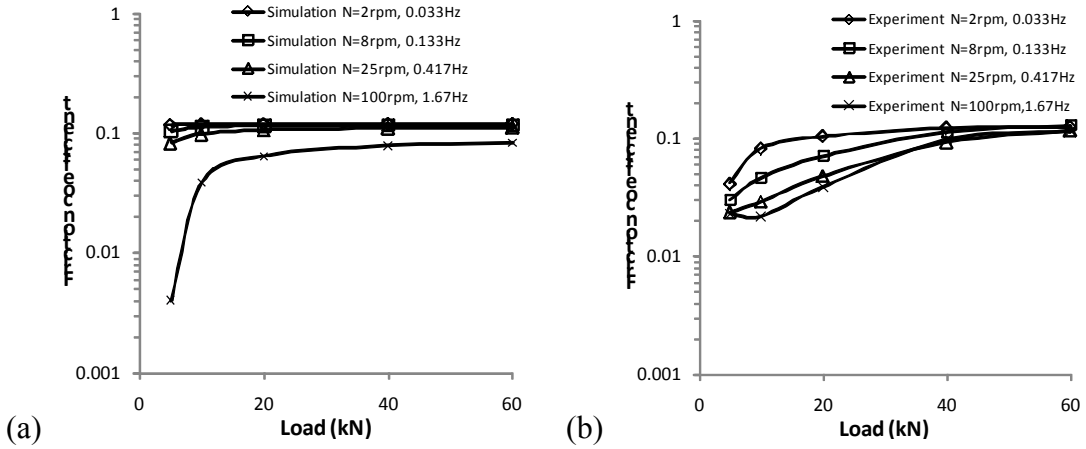

Figure 10 Friction coefficient against load (a) simulation, (b) experiment

Figure 11(a), Figure 12(a) and Figure 13(a) show the predicted torque cycle from the model for a full articulation of the pin joint. Figure 11(b), Figure 12(b) and Figure 13(b) show the experiment measurement of the same cycle. The cycles have similar form and magnitude. At higher speed there is some oscillation in the recorded torque. This is believed to be an effect of the hydraulic contact cannot respond quickly enough to the command signal.

As the lower speeds the torque during rotation remains virtually constant (another indication that hydrodynamic is negligible). At the higher speeds there is a reduction in torque as the joint articulates at its maximum velocity.

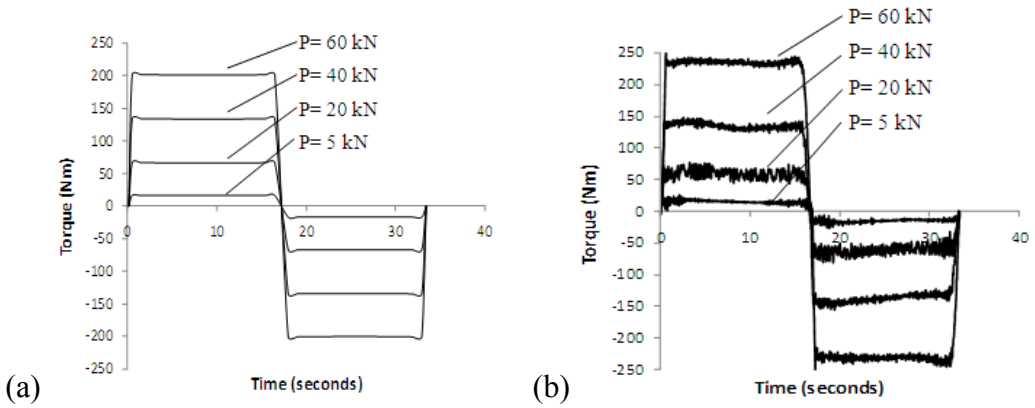

Figure 11 Frictional torque varying with time at f =0.03Hz (1.8rpm)

(a) simulation, (b) experiment

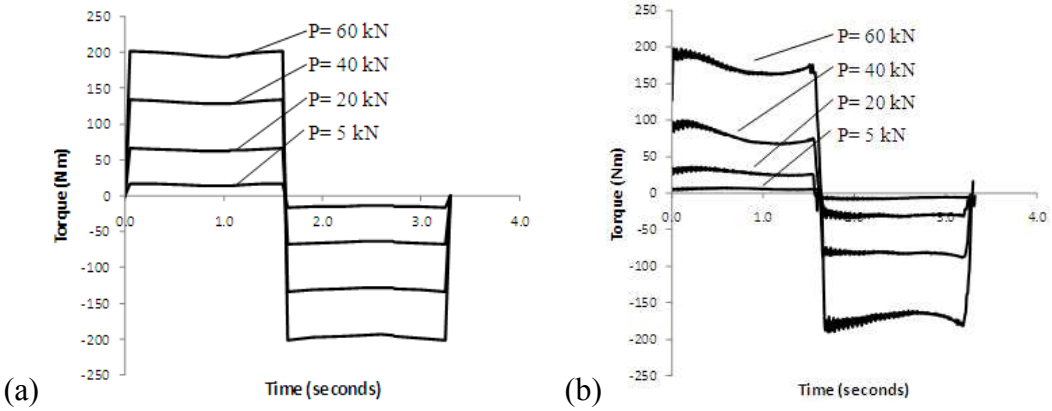

Figure 12 Frictional torque varying with time at f =0.3Hz (18rpm)

(a) simulation, (b) experiment

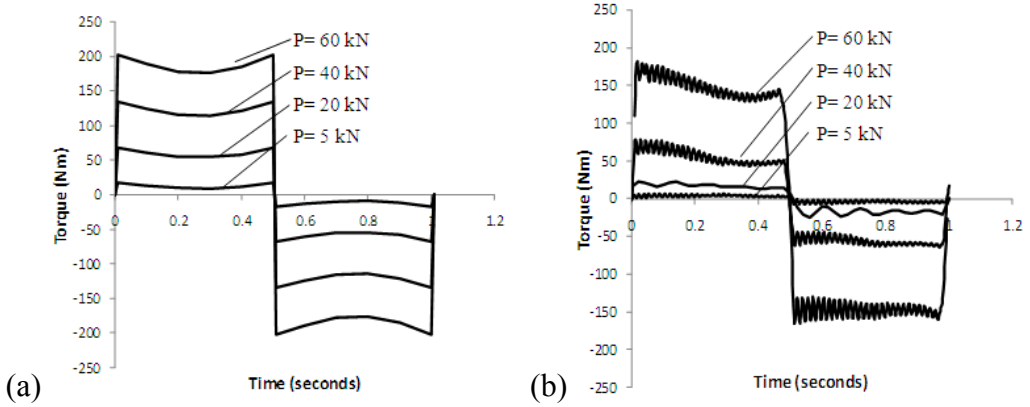

Figure 13 Frictional torque variation with time at f =1Hz (60rpm)

(a) simulation, (b) experiment

Conclusions

Pin joints, such as those in aircraft landing gear, are subjected to high load and slow speed. These conditions are not conducive to the formation of a separating lubricant

film and the joint operates with significant metallic contact. A mixed lubrication model of the pin and bush contact has been built to determine the torque during articulation in order to assist in the joint design and actuator sizing. Experiments were also performed on a purpose built apparatus to measure the torque during articulations of a pin and bush assembly under a range of load and speed condition.

Both the model and experiments demonstrate that for all practical purposes the pin joint operates in a boundary regime with hydrodynamic lift having little effect on the overall friction. Whilst the agreement between model and experiment is good, the model relies on prior knowledge of the 'dry' friction coefficient between asperities in contact. This parameter, and indeed the concept behind what actually is dry contact between asperities in a lubricated contact are difficult to determine.

Acknowledgement

The authors acknowledge the help and support of the Safran Group and Messier-Dowty Ltd and are grateful for their permission to publish.

Nomenclature

a half width of Hertzian contact

A contact area

B length of contact

c radial clearance

c_p constant in Roelands's formula

d_d distance between mean line of asperities and mean line of surface

E elastic modulus of pin

E_b elastic modulus of bush

E' reduced elastic modulus

f rotation frequency of pin

h film thicknes

n density of asperities

p contact pressure

P load

Q friction force

R radius of pin

R_b radius of bush

R' feduced radius

S Sommerfeld number

T friction torque

u velocity of contacting surfaces

Z Roelands' pressure-viscosity index

α pressure-viscosity coefficient

β average asperity radius

β_0 slope of the limiting shear stress-pressure relation

γ_1 proportion of load supported by fluid film

γ_2 proportion of load supported by asperity contact

λ film thickness parameter

η dynamic viscosity

η_0 lubricant viscosity at inlet temperature

η_∞ constant in Roelands's formula

μ friction coefficient

ν Poissons ratio of pin

ν_b Poissons ratio of bush

σ root mean square roughness of pin

σ_b root mean square roughness of bush

σ_s standard deviation of asperity summit heights

τ_L limiting shear stress

τ_{L0} limiting shear stress at ambient pressure

ω rotation velocity of pin

References

[1] Glaeser, W.A., and Dufrane, K.F., 1976, "*Performance of Heavily-loaded Oscillatory Journal Bearings*," ASLE Transactions, **20**, pp. 309-314.

[2] Glaeser, W.A., and Dufrane, K.F., 1975, "*Operating Limitations of Heavily Loaded Grease-Lubricated Cast Bronze Bearings*," Lubrication engineering, 31, pp.614-618.

[3] Lu, X., Khonsari, M. M., and GelinckE,. R. M., 2006, "*The Stribeck Curve: Experimental Results and Theoretical Prediction*," ASME J. Tribol., **128**, pp. 789-794.

[4] Greenwood, J. A., and Williamson, J. B. P., 1966, "*Contact of Nominally Flat Surfaces*," Proc. R. Soc. London, Ser. A, **295**, pp. 300-319.

[5] Moes, H., 1992, "*Optimum Similarity Analysis With Application to elastohydrodynamic Lubrication*," Wear, **159**, pp. 57-66.

[6] Johnson, K. L., Greenwood, J. A., and Poon, S. Y., 1972, "*A Simple Theory of Asperity Contact In Elastohydrodynamic Lubrication*," Wear, **19**, pp. 91-108.

[7] Bair, S., and Winer, W. O., 1979, "*A Rheological Model for EHL Contacts Based on Primary Laboratory Data*," ASME J. Lubr. Technol., **101**(3), pp. 258-265.

[8] Hamrock, B. J., August 2004, *Fundamentals of Fluid Film Lubrication*, Marcel Dekker Inc.

[9] Zhu, J., Pugh, S., Dwyer-Joyce, R. S., Beke, A., Cumner, G. and Ellaway, T., 2010, *"Experiments on the Pressure Distribution and Frictional Torque in Articulating Pin Joints,"* Proc. IMechE Part J: J. Engineering Tribology, **224**, pp.1153-1162.

[10]Colbert, R. S., Alvarez, L. A., Hamilton, M. A., Steffens, J. G., Ziegert, J. C., Burris, D. L., and Gregory Sawyer, W. 2010, *"Edges, Clearances, and Wear: Little Things that Make Big Differences in Bushing Friction,"* Wear, **268**(1–2), pp.41-49.

[11] Gelinck, E. R. M., and Schipper, D. J., 2000, "*Calculation of Stribeck Curves for Line Contacts*," Tribol. Int., **33**, pp. 175-181.

[12] Whitehouse, D. J., and Archard, J. F., 1970, "*The Properties of Random Surfaces of Significance in Their Contact*," Proc. R. Soc. London, Ser. A, **316**, pp. 97-121.

[13] Khonsari, M. M., and Hua, D. Y., 1994, "*Thermal Elastohydrodynamic Analysis Using a Generalized Non-Newtonian Formulation With Application to Bair-Winer Constitutive Equation*," ASME J. Tribol., **116**, pp. 37-45.

[14]Lunn, B., 1957, "*Friction and Wear under Boundary Lubrication:a Suggestion*," Wear, **1**, pp. 25-31.

[15] A. Cameron, *Basic Lubrication Theory*, Ellis Horwood Ltd, 1981.

[16] Stachowiak, G. W., and Batchelor, A. W., 2005, *Engineering Tribology (Third edition)*, Elsevier Inc., UK.